



## Article

# Structural and spectroscopic study of well-developed crystals of parahibbingite, $\beta$ -Fe<sub>2</sub>(OH)<sub>3</sub>Cl, formed from terrestrial weathering of the Muonionalusta iron meteorite

Simone Margheri<sup>1</sup>, Luca Bindi<sup>1,2\*</sup> , Paola Bonazzi<sup>1</sup> and Dan Holtstam<sup>3</sup> 

<sup>1</sup>Dipartimento di Scienze della Terra, Università degli Studi di Firenze, Via G. La Pira, 4 – I-50121 Firenze, Italy; <sup>2</sup>CNR-Istituto di Geoscienze e Georisorse, Sez. di Firenze, Via G. La Pira, 4 – I-50121 Firenze, Italy and <sup>3</sup>Department of Geosciences, Swedish Museum of Natural History, Box 50007, SE-104 05 Stockholm, Sweden

### Abstract

Parahibbingite [ $\beta$ -Fe<sub>2</sub>(OH)<sub>3</sub>Cl], a new mineral recently described from ultramafic rocks in the Bushveld Complex, South Africa, has been found to form millimetric well-developed crystals as a terrestrial weathering product of the Muonionalusta iron meteorite. The mineral, initially identified by means of Raman spectroscopy, was found in a small cavity within a crust of rust on a granitic rock fragment that was in direct contact with the alteration crust of a meteorite specimen, collected in the Kitkiöjärvi area, Sweden. Its crystal structure was refined from single-crystal X-ray diffraction data ( $R_1 = 0.0331$ ) in the space group  $R\bar{3}m$  [ $a = 6.9362(4)$ ,  $c = 14.673(1)$  Å and  $V = 611.35(7)$  Å<sup>3</sup> for  $Z = 6$ ], thus confirming the structural model of synthetic  $\beta$ -Fe<sub>2</sub>(OH)<sub>3</sub>Cl. It consists of a network of octahedrally coordinated Fe<sup>2+</sup> atoms alternately arranged in triangular and Kagomé layers, stacked along the  $c$  axis. The H atom position was determined, showing O–H...Cl bonds, which provides a further link between layers. Parahibbingite is found to be not only an important constituent of the corrosion system of archaeological iron artefacts but can also play an important role as an alteration product of iron meteorites.

**Keywords:** parahibbingite, Muonionalusta, iron meteorite, terrestrial weathering, single-crystal X-ray diffraction, micro-Raman spectroscopy, crystal structure, paratacamite, Sweden

(Received 26 May 2022; accepted 31 August 2022; Accepted Manuscript published online: 19 September 2022; Associate Editor: Charles A Geiger)

### Introduction

Parahibbingite corresponds to the  $\beta$ -form of ferrous-hydroxychloride, which was first synthesised and described by Oswald and Feitknecht (1964); since then, it has often been reported as a Cl-rich corrosion product of archaeological iron artefacts, and it has been the subject of numerous studies aimed at the conservation of archaeological objects (e.g. Réguer *et al.*, 2005, 2007a; Azoulay *et al.*, 2013).

Natural and anthropogenic specimens of the  $\beta$ -form of ferrous hydroxychloride typically occur as microcrystalline masses included in thin corrosion layers at the metal/oxide interface associated with akaganeite ( $\beta$ -FeOOH) (Réguer *et al.*, 2015), whereas synthetic samples are polycrystalline powders (Fujihala *et al.*, 2010).

The recent finding of microcrystalline aggregates among the alteration products recovered from a drill core from the Karee platinum mine in the Bushveld Complex, South Africa, allowed Koděra *et al.* (2022) to get parahibbingite approved by the International Mineralogical Association as a new species. The

new mineral occurred as fine-grained rims at the contact between orthopyroxene and talc, as a result of late hydrothermal alteration of pyroxenite.

In addition to the  $\beta$ -phase, ferrous hydroxychloride exhibits two other polymorphs:  $\alpha$  and  $\gamma$  (Oswald and Feitknecht, 1964). The metastable  $\alpha$ -Fe<sub>2</sub>(OH)<sub>3</sub>Cl (space group  $P\bar{3}m1$ ) has never been found in Nature (Koděra *et al.*, 2022). The natural  $\gamma$ -phase (space group  $Pnam$ ), named hibbingite, was first described by Saini-Eidukat *et al.* (1994) in a partially serpentinised troctolite from the Duluth Complex, Minnesota, USA, and since then it has been occasionally reported in both ore deposits and in the alteration crust of meteorites (e.g. Saini-Eidukat *et al.*, 1998; Pekov *et al.*, 2007; Zubkova *et al.*, 2019). However, due to its microcrystalline nature, it can be difficult to distinguish between  $\beta$ - and  $\gamma$ -Fe<sub>2</sub>(OH)<sub>3</sub>Cl. Furthermore, the name hibbingite has often been used incorrectly to refer to the  $\beta$ -phase (e.g. Buchwald and Koch, 1995; Simon *et al.*, 2018) and it is likely that some samples identified as hibbingite may actually be parahibbingite (Koděra *et al.*, 2022).

Nevertheless, Réguer *et al.* (2015) were able to recognise coexisting  $\beta$  and  $\gamma$  phases occurring in archaeological iron corroded in a marine environment by means of powder X-ray diffraction. In addition, these two phases can be easily distinguished via Raman spectroscopy (Koděra *et al.*, 2022).

\*Author for correspondence: Luca Bindi, Email: [luca.bindi@unifi.it](mailto:luca.bindi@unifi.it)

Cite this article: Margheri S., Bindi L., Bonazzi P. and Holtstam D. (2022) Structural and spectroscopic study of well-developed crystals of parahibbingite,  $\beta$ -Fe<sub>2</sub>(OH)<sub>3</sub>Cl, formed from terrestrial weathering of the Muonionalusta iron meteorite. *Mineralogical Magazine* 86, 891–896. <https://doi.org/10.1180/mgm.2022.108>

The recent occurrence of exceptionally well-crystallised parahibbingite associated with a fragment of the Muonionalusta iron meteorite from northernmost Sweden (Wickman, 1964; Buchwald, 1975) allowed us to carry out a single-crystal X-ray diffraction study and collect high-quality micro-Raman data from the mineral.

### Occurrence

The Muonionalusta meteorite consists of a collection of a large number of fragments, ranging from 0.04 up to 1200 kg, found in a wide area (25 × 15 km) centred around lake Kitkiöjärvi, Pajala District, Norrbotten County, Sweden. It is deemed that the original body of the Muonionalusta meteorite did not hit the ground as a single impactor, but exploded mid-air, creating a meteorite shower (Wickman, 1964; Lagerbäck and Wickman, 1997). The meteorite fragments have experienced at least one glacial period (the Weichselian, 115 to 12 ka), and associated glacial transport processes could be responsible, along with the impact dynamic, for the considerable size of the present distribution area (Hättestrand, 2009).

The Muonionalusta meteorite belongs to group IVA and consists mainly of Fe–Ni alloys forming a fine octahedrite texture and containing polycrystalline troilite nodules and minor amounts of daubréelite, chromite and schreibersite (Buchwald, 1975). It is the first iron meteorite in which stishovite has been reported, probably formed during shock metamorphism in space of primary tridymite (Holtstam *et al.*, 2003).

Fragments of the meteorite are generally found at different depths in tillite beds, sometimes intermingled with glaciofluvial sediments, and are usually covered by a crust of rusty material, which commonly includes fragments of the surrounding soil. The crust is populated by a wide variety of alteration products, mainly iron oxides, oxyhydroxides and hydroxychloride, such as magnetite, maghemite, goethite, akaganeite, lepidocrocite, and the recently approved mineral muonionalustaitaite [Ni<sub>3</sub>(OH)<sub>4</sub>Cl<sub>2</sub>·4H<sub>2</sub>O] (Holtstam *et al.*, 2020).

Parahibbingite has been found in a small cavity of rust crust on a 9 × 7 × 4 cm granitic rock fragment associated with the alteration crust of the meteorite (sample GEO-NRM #20060957). The fragment was in direct contact with a 22 kg specimen of the Muonionalusta meteorite, recovered from a depth of 1.4 m, ca 5 km NE of Kitkiöjärvi. The cavity was found to be filled with an unknown brownish liquid when it was opened in the field.

Parahibbingite forms well-developed crystals (transparent with a greenish tinge) up to 2 mm in size, and is covered by a reddish-brown rim of akaganeite (Fig. 1). In the same cavity, brownish-orange hexagonal-shaped lamellae of an unknown Fe- and sulfate-bearing phase have been found. Despite their distinct morphology, these lamellae turned out to be a poorly crystallised phase which is still under investigation. It is likely that at least partly, some of the akaganeite in the present sample formed during atmospheric oxidising post-excavation conditions (since 2006).

### X-ray crystallography and structure refinement

Several crystal fragments of parahibbingite, ranging from 0.1 up to 0.2 mm in size, were examined by means of a D8 Advance diffractometer equipped with a Photon III detector, using graphite-monochromatised MoK $\alpha$  radiation ( $\lambda = 0.71073$  Å). The unit-cell values were nearly identical for all the crystals tested. Intensity data collection was carried out on the crystal showing the best diffraction quality [unit-cell parameters:  $a = 6.9362(4)$ ,  $c = 14.673(1)$  Å and  $V = 611.35(7)$  Å<sup>3</sup>]. Intensities were corrected



**Fig. 1.** Mineral association consisting of parahibbingite crystals covered with a reddish-brown coating of akaganeite, and brownish-orange lamellae of an unknown, poorly crystallised phase. Field of view = 6 mm. Picture courtesy of Torbjörn Lorin, private collection.

for Lorentz and polarisation factors and absorption using the software package *APEX3* (Bruker, 2016).

The merging factor in the Laue group  $\bar{3}m$  ( $R_{\text{int}} = 0.040$ ), reflection conditions ( $hkl: -h+k+l = 3n$ ) and the statistical tests on the distribution of  $|E|$  values ( $|E^2 - 1| = 0.917$ ) suggested the space group  $R\bar{3}m$ , in accord with that determined for the synthetic samples. Therefore, the structure was refined starting from the atomic coordinates reported for synthetic  $\beta\text{-Fe}_2(\text{OH})_3\text{Cl}$  (Réguer *et al.*, 2015) using the program *Shelxl-2013* (Sheldrick, 2015). The site occupancy factor (s.o.f.) at the cation sites was allowed to vary (Fe vs. structural vacancy for the two octahedral sites) using scattering curves for neutral atoms taken from the *International Tables for Crystallography* (Wilson, 1992). Two sites (Wyckoff positions  $3b$  and  $9e$ , labelled Fe1 and Fe2 respectively) were found to be fully occupied by Fe atoms and thus their occupancy was fixed in the successive least-squares cycles and an anisotropic model of the whole structure was refined.

Convergence was achieved quickly to  $R_1 = 0.0335$  for 320 observed reflections [ $F_o^2 > 4\sigma(F_o^2)$ ] and 0.0501 for all 402 independent reflections. At this stage, the inspection of the  $\Delta F$ -map showed a significant residual peak of  $\approx 2 e^-/\text{Å}^3$  at  $\sim 0.95$  Å from the oxygen atom, that was attributed to an H atom. The introduction of this additional peak slightly improved the  $R$  indices [ $R_1 [F_o^2 > 4\sigma(F_o^2)] = 0.0331$ ,  $R_1 = 0.0496$ ]. Nevertheless, the  $U_{\text{iso}}$  of the hydroxyl H atom had a too high value, so the H atom was refined using a riding model with  $U_{\text{iso}}(\text{H}) = 1.5 \times U_{\text{eq}}(\text{O})$  and the O–H distance restrained to 0.90(2) Å.

Experimental details are reported in Table 1. Fractional atomic coordinates and anisotropic-displacement parameters are given in Table 2 and 3, respectively. Selected bond distances, angles and bond valence sums are given in Table 4. Further details of the crystal structure investigations and the list of the observed and calculated structure factors may be obtained from the crystallographic information file deposited with CCDC/FIZ Karlsruhe online deposition service [<https://www.ccdc.cam.ac.uk/structures/> under the deposition number CSD-2192582] or with Supplementary material (see below).

### Micro-Raman investigation

A micro-Raman spectrum of parahibbingite (Fig. 2) was collected from a polished crystal on a LabRAM HR 800 micro-spectrometer,

**Table 1.** Data and experimental details.

Crystal data	
Ideal formula	Fe <sub>2</sub> (OH) <sub>3</sub> Cl
Crystal system	Trigonal
Space group	<i>R</i> $\bar{3}m$
<i>a</i> (Å)	6.9362(4)
<i>c</i> (Å)	14.673(1)
<i>V</i> (Å <sup>3</sup> )	611.35(9)
<i>Z</i>	6
Data collection	
Crystal size (mm)	0.10×0.07×0.08
Diffractionmeter	D8 Advance
Distance to detector (cm)	7
Scan modes	$\omega/\varphi$
Exposure time per frame (s)	20
Radiation type	MoK $\alpha$ ( $\lambda = 0.71073$ Å)
Temperature (K)	293
Collected reflections	1616
Unique reflections	402
Reflections with $F_o^2 > 4\sigma(F_o^2)$	320
2 $\theta$ range (°)	4.2–36.8
<i>R</i> <sub>int</sub>	0.040
Refinement	
Refinement	Full-matrix least-squares on $F^2$
Number of least-squares parameters	18
<i>wR</i> <sub>2</sub>	0.0770
Final <i>R</i> <sub>1</sub> [ $F_o^2 > 4\sigma(F_o^2)$ ]	0.0331
Final <i>R</i> <sub>1</sub>	0.0495
Goof	1.098
$\Delta\rho_{\max}, \Delta\rho_{\min}$ (e <sup>-</sup> /Å <sup>3</sup> )	1.35, -1.11

$R_{int} = \sum |F_o^2 - F_o^2(\text{mean})| / \sum |F_o^2|$ .  $Goof = S = \{ \sum [w(F_o^2 - F_c^2)^2] / (n - p) \}^{1/2}$ , where *n* = no. of reflections, *p* = no. of refined parameters.  $R_1 = \sum ||F_o| - |F_c|| / \sum |F_o|$ .  $wR_2 = \{ S [w(F_o^2 - F_c^2)^2] / S [w(F_o^2)^2] \}^{1/2}$ ;  $w = 1 / [\sigma^2(F_o^2) + (0.340P)^2]$  where  $P = [F_o^2 + 2(F_c^2)]/3$ .

using a 514 nm Ar-ion laser source at 1 mW power, a peltier-cooled (-70°C) CCD detector (Synapse), Olympus objective (magnification 100/ numerical aperture 0.9) and laser spot of ~3 μm. Spectral positions were corrected against the Raman band at 789 cm<sup>-1</sup> of pure SiC-6H on {0001}. The spectral resolution is ~1 cm<sup>-1</sup>. Instrument control and data acquisition (range 100–4000 cm<sup>-1</sup>) were made with the *LabSpec 5* software. The specimen showed no sign of degradation under the laser beam during measurement.

In the spectrum obtained, Raman bands are detected at 3565, 3553, 810, 618, 428, 321, 202, 163 and 127 cm<sup>-1</sup>. The positions agree within ±5 cm<sup>-1</sup> with data for β-Fe<sub>2</sub>(OH)<sub>3</sub>Cl obtained from the corrosion product of a 15<sup>th</sup> Century nail (Réguer *et al.*, 2007b) and with the recent data for parahibbingite (Koděra *et al.*, 2022). Compared to previous measurements, our spectrum is free from contributions from admixed impurities and has a considerably lower noise level. Following the assignments of Réguer *et al.* (2007b), the two strongest bands at ~3660 cm<sup>-1</sup>

**Table 2.** Atoms, Wyckoff positions, atomic coordinates and atomic displacement parameters for the structure of parahibbingite.

Atom	Wyckoff	<i>x</i>	<i>y</i>	<i>z</i>	<i>U</i> <sub>iso</sub> <sup>*</sup> / <i>U</i> <sub>eq</sub>
Fe1	3 <i>b</i>	0	0	½	0.0135(2)
Fe2	9 <i>e</i>	½	0	0	0.01451(17)
Cl	6 <i>c</i>	0	0	0.21651(8)	0.0172(4)
O	18 <i>h</i>	0.20145(19)	0.79855(19)	0.06872(15)	0.0168(2)
H	18 <i>h</i>	0.136(2)	-0.136(2)	0.088(2)	0.025(3) <sup>*</sup>

<sup>\*</sup>The isotropic displacement parameter of the H atom was fixed during the refinement (see text).

**Table 3.** Anisotropic displacement parameters for the structure of parahibbingite.

	<i>U</i> <sup>11</sup>	<i>U</i> <sup>22</sup>	<i>U</i> <sup>33</sup>	<i>U</i> <sup>12</sup>	<i>U</i> <sup>13</sup>	<i>U</i> <sup>23</sup>
Fe1	0.0149(3)	<i>U</i> <sup>11</sup>	0.0105(4)	0.00747(14)	0	0
Fe2	0.0147(2)	0.0129(3)	0.0153(3)	0.00646(13)	0.00122(10)	0.0024(2)
Cl	0.0187(3)	<i>U</i> <sup>11</sup>	0.0140(5)	0.00937(17)	0	0
O	0.0182(7)	<i>U</i> <sup>11</sup>	0.0167(10)	0.0112(8)	0.0006(4)	- <i>U</i> <sup>13</sup>

are related to OH-stretching vibration modes. Multiple bands in the region 300–700 cm<sup>-1</sup> are ascribed to Fe–Cl and Fe–O stretching modes. The band at ~810 cm<sup>-1</sup> belongs to a hydroxyl deformation mode (Réguer *et al.*, 2007b), whereas the one at 163 cm<sup>-1</sup> corresponds to bending of O–Fe–O bonds. The relatively strong peak at 127 cm<sup>-1</sup> is tentatively assigned to lattice modes.

As regards the two bands in the OH region, they also appear in the spectra of previous papers at almost the same positions. Réguer *et al.* (2007b) supposed that the two major hydroxyl stretching bands could be related to two crystallographically independent hydroxyl groups. For this reason, we carried out structural refinements at lower symmetries than *R* $\bar{3}m$  (starting from *R* $\bar{3}$ ) and also tried to refine O-versus-Cl occupancies at both anionic positions, but no indication of possible mixed occupancies was found thus leading to the conclusion that there are not different hydrogen environments. Alternatively the split of vibration bands observed in the Raman spectrum could be related to chemical substitutions at the octahedral sites which would create slightly different surroundings, i.e. next-nearest-neighbour effects. However, from previous microchemical (SEM-EDS) data, we know that the maximum metal impurity is *ca.* 0.05 apfu of Co, and this is not expected to create a significant effect.

### Description of the structure and discussion

The crystal structure of parahibbingite (Fig. 3) can be described as a stacking along the *c* axis of two different types of layers, made of octahedrally coordinated Fe<sup>2+</sup> atoms. In one layer, iron cations are arranged in Kagomé planes [Fe2 atoms, Fig. 3a], while in the

**Table 4.** Selected bond distances (Å), angles (°) and bond valence sums (BVS) for the structure of parahibbingite.

Fe1 (BVS = 2.01)		Fe2 (BVS = 2.02)	
Fe1–O (×6)	2.139(2)	Fe2–O ×4	2.0890(12)
$\sigma^2$	113.5	Fe2–Cl ×2	2.6358(8)
$\lambda$	1.029	$\sigma^2$	60.8
O–Fe1–O ×3	180	$\lambda$	1.042
O–Fe1–O ×6	79.81(9)	O–Fe2–Cl ×4	82.75(5)
O–Fe1–O ×6	100.20(9)	O–Fe2–Cl ×4	97.25(5)
		O–Fe2–O ×2	180
Fe1–Fe2	3.1607(2)	O–Fe2–O ×2	97.88(12)
Fe2–Fe2	3.4681(3)	O–Fe2–O ×2	82.12(13)
		Cl–Fe2–Cl ×1	180
H (BVS = 0.93)			
O (BVS = 1.98)			
Cl (BVS = 0.88)			
O–H	0.86(2)		
Cl...H	2.48(3)		
O–H...Cl	149(3)		

The mean quadratic elongation ( $\lambda$ ) and the angle variance ( $\sigma^2$ ) were computed according to Robinson *et al.* (1971); the bond valence sums (BVS) were calculated according to the parameters of Brese and O’Keeffe (1991).

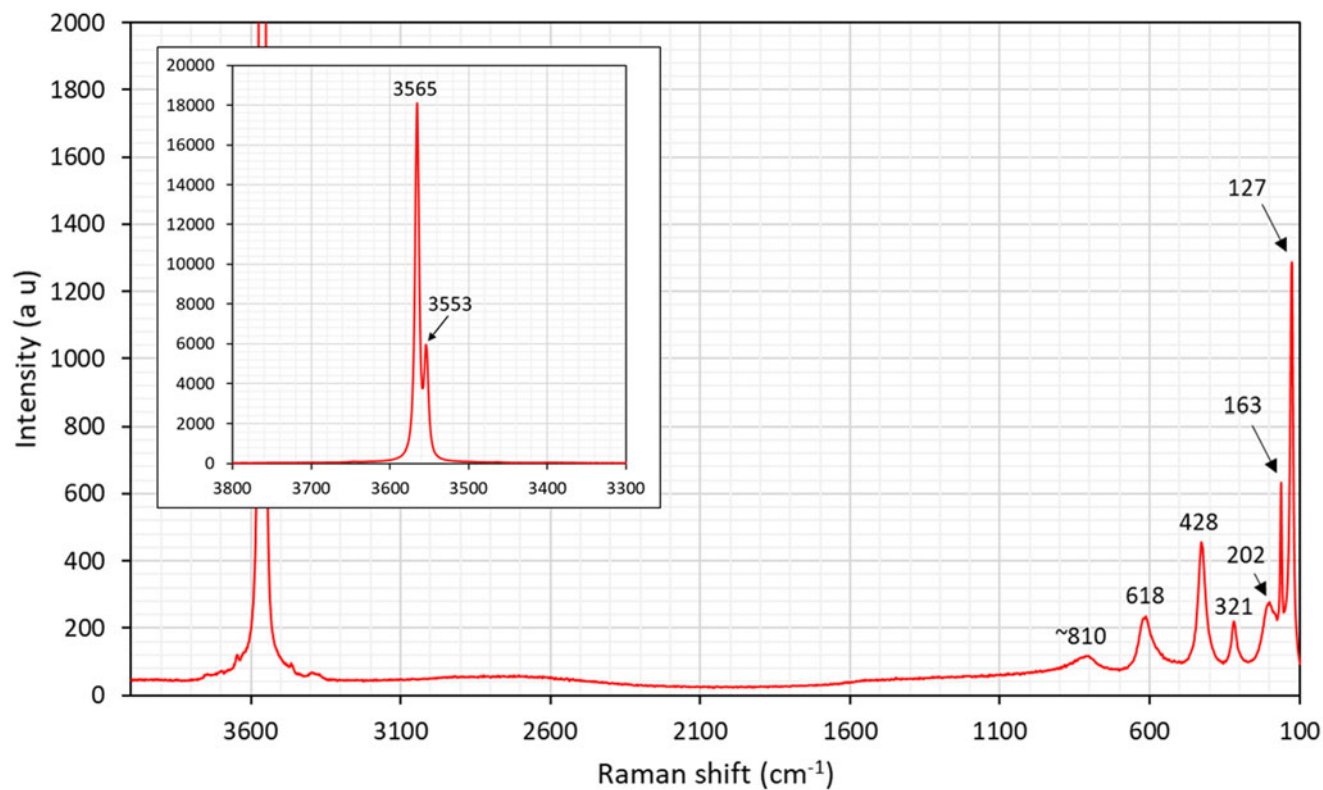


Fig. 2. Micro-Raman spectrum of parahibbingite obtained with a 514 nm laser.

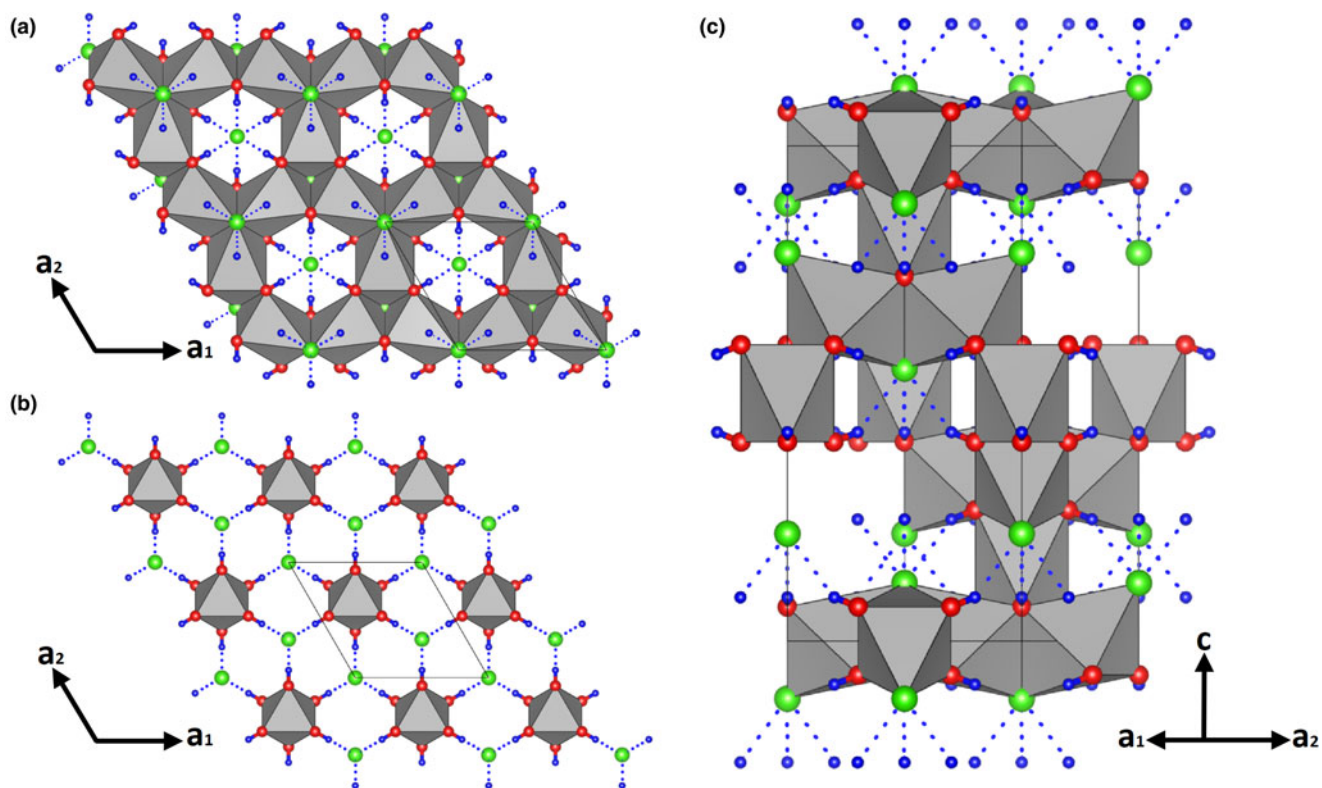


Fig. 3. The crystal structure of parahibbingite. (a) Kagomé planes and (b) triangular planes seen down the  $c$  axis. (c) View along the  $c$  axis. Colour scheme: Fe = grey; Cl = green; O = red; H = blue.  $\text{H}\cdots\text{Cl}$  bridges are indicated as dashed lines. Drawn using *Vesta* (Momma and Izumi, 2011).

other layer, they are disposed in triangular planes [Fe1 atoms, Fig. 3b].

$\text{Fe1O}_6$  octahedra are disjointed from each other, but they share O–O edges with  $\text{Fe2O}_4\text{Cl}_2$  polyhedra of the upper and lower layers, while  $\text{Fe2O}_4\text{Cl}_2$  octahedra are joined in interconnected triplets sharing a Cl–O edge. Each chlorine atom acts as acceptor of three H bonds from the oxygen atom (dotted lines in Fig. 3c), thus reaching a bond valence sum close to 1 (Table 4). These O–H...Cl bonds provide further linking between Kagomé and triangular planes.

Parahibbingite is isostructural with herbertsmithite,  $\text{Cu}_3\text{Zn}(\text{OH})_6\text{Cl}_2$  (Braithwaite *et al.*, 2004), gillardite,  $\text{Cu}_3\text{Ni}(\text{OH})_6\text{Cl}_2$  (Clissold *et al.*, 2007), tonidite,  $\text{Cu}_3\text{Mg}(\text{OH})_6\text{Cl}_2$  (Malcherek *et al.*, 2014) and leverettite (Kampf *et al.*, 2013). The unit cell of these minerals is also analogous to the subcell of paratacamite [ $\text{Cu}_2(\text{OH})_3\text{Cl}$ ] (Welch *et al.*, 2014). The slight differences between parahibbingite and the above-mentioned mineral structures are mainly due to the different nature of the cations at the octahedral sites.

The origin of parahibbingite crystals from the weathered Muonionalusta iron meteorite is unclear. Specimens from Bushveld Complex seem to form as a result of late hydrothermal processes: divalent iron from orthopyroxene reacted with  $\text{Cl}^-$  in hydrothermal fluids creating a thin reaction rim on orthopyroxene phenocrysts. The textural relationships with other minerals suggest that parahibbingite formed after talc and amphibole, which are the earliest alteration products of the original pyroxenite (Kodéra *et al.*, 2022). In the present case, the formation process of parahibbingite associated with an iron meteorite could be similar to those involved in the alteration of archaeological iron artefacts. Similarly to the alteration products of anthropogenic objects, iron originates directly from the alloy. In this light, the iron in parahibbingite studied here most probably stems from the meteoritic Fe–Ni alloy, whereas chlorine may have been provided from the surrounding environment. Cl concentrations in the local soil are in fact remarkably high, because of the presence of significant amounts of Cl-bearing minerals, mainly scapolite- and apatite-group minerals, in the underlying bedrock (Ladenberger *et al.*, 2012; Holtstam *et al.*, 2020). In addition, the long time of residence in a relatively stable and protected anoxic environment may have played an important role in the formation of large single crystals with a good degree of crystallinity. Kodéra *et al.* (2022) hypothesised that the  $\beta$ -form is actually the most stable polymorph of  $\text{Fe}_2(\text{OH})_3\text{Cl}$  at ambient temperatures.

**Acknowledgments.** The paper benefited by the careful insights of two anonymous reviewers and the comments by the Structural Editor Peter Leverett. This research received support by Ministero dell'Istruzione, dell'Università e della Ricerca through the project PRIN 2017 "TEOREM – deciphering geological processes using Terrestrial and Extraterrestrial ORE Minerals", prot. 2017AK8C32 (PI: Luca Bindi). Thanks are due to Anders Zetterqvist and Torbjörn Lorin for providing Muonionalusta specimens to the Swedish Museum of Natural History.

**Supplementary material.** To view supplementary material for this article, please visit <https://doi.org/10.1180/mgm.2022.108>.

**Competing interests.** The authors declare none.

## References

Azoulay I., Conforto E., Refait P. and Rémazeilles C. (2013) Study of ferrous corrosion products on iron archaeological objects by electron backscattered diffraction (EBSD). *Applied Physics*, **A110**, 379–388.

- Braithwaite R.S.W., Mereiter K., Paar W.H. and Clark A.M. (2004) Herbertsmithite,  $\text{Cu}_3\text{Zn}(\text{OH})_6\text{Cl}_2$ , a new species, and the definition of paratacamite. *Mineralogical Magazine*, **68**, 527–539.
- Brese N.E. and O'Keeffe M. (1991) Bond valence parameters for solids. *Acta Crystallographica*, **B47**, 192–197.
- Bruker (2016) APEX3, SAINT, and SADABS. Bruker AXS Inc., Madison, Wisconsin, USA.
- Buchwald V.F. (1975) *Handbook of Iron Meteorites. Their History, Distribution, Composition and Structure*. Arizona State University, USA, 1426 pp.
- Buchwald V.F. and Koch C.B. (1995) Hibbingite ( $\beta\text{-Fe}_2(\text{OH})_3\text{Cl}$ ), a chlorine-rich corrosion product in meteorites and ancient iron objects. *Meteoritics*, **30**, 493–494.
- Clissold M.E., Leverett P. and Williams P.A. (2007) The structure of gillardite, the Ni-analogue of herbertsmithite, from Widgiemooltha, Western Australia. *The Canadian Mineralogist*, **45**, 317–320.
- Fujihala M., Hagihala M., Zheng X.G. and Kawae T. (2010) Antiferromagnetic magnetic transition and spin fluctuations in the deformed pyrochlore compound  $\beta\text{-Fe}_2(\text{OH})_3\text{Cl}$ . *Physical Review B*, **82**, 024425.
- Hättestrand C. (2009) Sprängd dvärgplanet i nordsvensk myrmark. *Forskning och framsteg*, **2009**(3), 46–51.
- Holtstam D., Broman C., Söderhielm J. and Zetterqvist A. (2003) First discovery of stishovite in an iron meteorite. *Meteoritics and Planetary Science*, **38**, 1579–1583.
- Holtstam D., Bindi L., Karlsson A., Söderhielm J. and Zetterqvist A. (2020) Muonionalustaitite,  $\text{Ni}_3(\text{OH})_4\text{Cl}_2\cdot 4\text{H}_2\text{O}$ , a new mineral formed by terrestrial weathering of the Muonionalusta iron (IVA) meteorite, Pajala, Norrbotten, Sweden. *GFF*, **143**, 1–7.
- Kampf A.R., Sciberras M.J., Williams P.A., Dini M. and Molina Donoso A.A. (2013) Leverettite from the Torrecillas mine, Iquique Province, Chile: the Co-analogue of herbertsmithite. *Mineralogical Magazine*, **77**, 3047–3054.
- Kodéra P., Majzlan J., Pollok K., Kiefer S., Šimko F., Scholtzová E., Luptáková J. and Cawthorn G. (2022) Ferrous hydroxychloride hibbingite ( $\gamma\text{-Fe}_2(\text{OH})_3\text{Cl}$ ) and parahibbingite ( $\beta\text{-Fe}_2(\text{OH})_3\text{Cl}$ ) as a concealed sink of Cl and  $\text{H}_2\text{O}$  in ultrabasic and granitic systems. *American Mineralogist*, **107**, 826–841.
- Ladenberger, A., Andersson, M., Gonzalez, J., Lax, K., Carlsson, M., Ohlsson, S.Å. and Jelinek, C. (2012) Markgeokemiska kartan. Morängekemik i norra Norrbotten. *Sveriges geologiska undersökning*, **K410**, 1–112.
- Lagerbäck R. and Wickman F.E. (1997) A new iron meteorite from Muonionalusta, northernmost Sweden. *GFF*, **119**, 193–198.
- Malcherek T., Bindi L., Dini M., Ghiara M.R., Molina Donoso A., Nestola F., Rossi M. and Schlüter J. (2014) Tonidite,  $\text{Cu}_3\text{Mg}(\text{OH})_6\text{Cl}_2$ , the Mg-analogue of herbertsmithite. *Mineralogical Magazine*, **78**, 583–590.
- Momma K. and Izumi F. (2011) VESTA 3 for three-dimensional visualization of crystal, volumetric and morphology data. *Journal of Applied Crystallography*, **44**, 1272–1276.
- Oswald H.R. and Feitknecht W. (1964) Über die Hydroxidhalogenide  $\text{Me}_2(\text{OH})_3\text{Cl}$ ,  $\text{Me}_2(\text{OH})_3\text{Br}$ , J zweiwertiger Metalle ( $\text{Me} = \text{Mg}, \text{Ni}, \text{Co}, \text{Cu}, \text{Fe}, \text{Mn}$ ). *Helvetica Chimica Acta*, **30**, 272–289.
- Pekov I.G., Perchiazzi N., Merlino S., Kalachev V.N., Melrini M. and Zadov A.E. (2007) Chukanovite,  $\text{Fe}_2(\text{CO}_3)(\text{OH})_2$ , a new mineral from the weathered iron meteorite Dronino. *European Journal of Mineralogy*, **19**, 891–898.
- Réguer S., Dillmann P., Mirambet F. and Bellot-Gurlet L. (2005) Local and structural characterisation of chlorinated phases formed on ferrous archaeological artefacts by  $\mu\text{XRD}$  and  $\mu\text{XANES}$ . *Nuclear Instruments and Methods in Physics Research B*, **240**, 500–504.
- Réguer S., Dillmann P. and Mirambet F. (2007a) Buried iron archaeological artefacts: Corrosion mechanisms related to the presence of Cl-containing phases. *Corrosion Science*, **49**, 2726–2744.
- Réguer S., Neff D., Bellot-Gurlet L. and Dillmann P. (2007b) Deterioration of iron archaeological artefacts: micro-Raman investigation on Cl-containing corrosion products. *Journal of Raman Spectroscopy*, **38**, 389–397.
- Réguer S., Mirambet F., Rémazeilles C., Vantelona D., Kergourlaya F., Neff D. and Dillmann P. (2015) Iron corrosion in archaeological context: Structural refinement of the ferrous hydroxychloride  $\beta\text{-Fe}_2(\text{OH})_3\text{Cl}$ . *Corrosion Science*, **100**, 589–598.
- Robinson K., Gibbs G.V. and Ribbe P.H. (1971) Quadratic elongation: a quantitative measure of distortion in coordination polyhedra. *Science*, **172**, 567–570.

- Saini-Eidukat B., Kucha H. and Keppler H. (1994) Hibbingite,  $\gamma\text{-Fe}_2(\text{OH})_3\text{Cl}$ , a new mineral from the Duluth Complex, Minnesota, with implications for the oxidation of Fe-bearing compounds and the transport of metals. *American Mineralogist*, **79**, 555–561.
- Saini-Eidukat B., Rudashevsky N.S. and Polozov A.G. (1998) Evidence for hibbingite–kempite solid solution. *Mineralogical Magazine*, **62**, 251–255.
- Sheldrick, G.M. (2015) Structure refinement with SHELXL. *Acta Crystallographica*, **C71**, 3–8.
- Simon H., Cibin G., Robbins P., Day S., Tang C., Freestone I. and Schofield E. (2018) A synchrotron-based study of the Mary Rose iron cannonballs. *Angewandte Chemie International Editions*, **57**, 7390–7395.
- Welch M.D., Sciberras M.J., Williams P.A., Leverett P., Schlueter J. and Malacherek T. (2014) A temperature-induced reversible transformation between paratacamite and herrbertsmithite. *Physics and Chemistry of Minerals*, **41**, 33–48.
- Wickman F.E. (1964) The Muonionalusta iron meteorites. *Arkiv för Mineralogi och Geologi*, **3**, 467–478.
- Wilson A.J.C. (1992) *International Tables for Crystallography*. Volume C: Mathematical, Physical and Chemical Tables. Kluwer Academic Publishers, Amsterdam.
- Zubkova, N.V., Pekov, I.V., Sereda, E.V., Yapaskurt, V.O. and Pushcharovsky, D.Yu. (2019) The crystal structure of hibbingite, orthorhombic  $\text{Fe}_2\text{Cl}(\text{OH})_3$ . *Zeitschrift für Kristallographie*, **234**, 379–382.